

Research on novel pressurized fiber Bragg grating static level based on circular structure*

XIANG Shaojun¹, LI Yang¹, XIA Zhiyin², and YANG Yan^{3**}

1. China Communications Construction Company Second Highway Consultants Co., Ltd., Wuhan 430056, China

2. School of Precision Instrument and Opto-electronics Engineering, Tianjin University, Tianjin 300072, China

3. National Engineering Research Center of Fiber Optic Sensing Technology and Networks, Wuhan University of Technology, Wuhan 430070, China

(Received 4 October 2022; Revised 30 January 2023)

©Tianjin University of Technology 2023

The static levelling system has significant value in the settling measurement of the structures. A novel pressurized static level based on circular structure is designed by using fiber Bragg grating (FBG) sensing technology in this research. The variation of the level pressure in the connecting vessel can be transmitted through the diaphragm to the FBG of the circular ring. The Ritz method is used to calculate the lateral deformation of the circular ring under the concentrated force, constructing the theoretical sensitivity model of the sensor. Further, finite element simulation and static experiments are applied to modify and verify it. According to the experimental data, two FBGs arranged horizontally along the circular ring, multiplying the sensitivity of the FBG static level to about 4.75 pm/mm, while the resolution can reach 0.02 mm. In addition, the temperature compensation of the sensor can be realized by the synergistic change of the measurement point and the reference point within the system of connecting vessel.

Document code: A **Article ID:** 1673-1905(2023)06-0321-6

DOI <https://doi.org/10.1007/s11801-023-2163-5>

Settling phenomena can cause damage to buildings and municipal facilities. To measure the settlement of the structure, static levels are positioned at the reference and monitoring points. According to the principle of connecting vessels, the sensor accurately identifies the variation in level height when the monitoring point is deformed vertically with respect to the reference. The measured system based on static level has been widely used in the field of settling monitoring of engineering structures^[1].

The sensing technology of fiber Bragg grating (FBG) has a promising application in structural health monitoring due to its multiple advantages of anti-interference, lightweight, passive device and high accuracy^[2]. At present, the structure of the studied FBG static levels is mainly floating cylinder type^[3]. The FBG static level of floating cylinder consisted of FBG, sensitive elements, float and rigid rod^[4]. The principle was to measure the buoyancy applied to the float, analyzing the variation of level height in the system. VORATHIN et al^[5] chose the cantilever beam as the sensitive element of FBG static level using the polyvinyl chloride (PVC) polymer to improve the sensitivity. RODRIGUES et al^[6] considered the channel steel structure to avoid the chirping phenomenon of FBG. However, based on the buoyancy principle, the lateral size of the floating cylinder must be

enlarged to increase the buoyancy, enhancing the sensitivity of the sensor at the same depth of immersion. The height of the internal chamber within the FBG static level of the floating cylinder must be larger than the range of the settlement, resulting in its integral volume being larger. In addition, the floating cylinder structure also has the disadvantages of being difficult to apply in vibration environment testing, with greater moisture evaporation^[3].

The settlement of the structure not only makes the level height of the connecting vessel vary, but also cause the variation of the level pressure at the monitoring point. Using the arrangement solution of pressure sensor can also detect the phenomenon of settlement, completely overcome the disadvantages of the floating cylinder type. Further, the monitoring points within the connecting vessel system are set up to be sealed when not connected to the atmosphere. Only the reservoir at the reference point is connected to the atmosphere. Some scholars had designed the corresponding static level considering the technique of Mach-Zehnder interferometer, Fabry-Perot interferometer, tilted FBG and chirped FBG with high sensitivity response to pressure^[7,8]. However, the immaturity of the demodulation technology led to low accuracy of the settlement. Regarding the FBG sensing technique, PACHAVA et al^[9] considered pasting the FBG in a circular diaphragm with the boundary. AMEEN et al^[10]

* This work has been supported by the Fundamental Research Funds for the Central Universities (No.205214001).

** E-mail: yangyan08@whut.edu.cn

encapsulated the FBG between a rubber diaphragm and a plastic diaphragm with low elastic modulus. Multiple hinges were designed by LIU to amplify the FBG sensitivity using the lever effect^[11]. But the sensitivity of all the above sensors is lower than 1 pm/mm, which cannot meet the requirement of accurate measurement.

In this paper, a novel pressurized FBG static level based on a circular structure and deformed diaphragm was proposed, which can realize the settling monitoring of structure and temperature compensation of sensor by using the principle of connecting vessel. The Ritz method and finite element analysis were used to establish the sensitivity model of the circular sensor which provided theoretical guidance for the design of the same type sensor. Based on the principle that the level pressure measures settlement, the designed circular FBG static level has the characteristics of miniaturization, strong anti-interference ability and minimal water evaporation, which can realize long-term monitoring. The volume of the encapsulated FBG static level was approximately $\phi 46 \text{ mm} \times 70 \text{ mm}$, which was much smaller than the current floating cylinder structure^[3-6]. The parallel arrangement of two FBGs not only multiplied the sensitivity of the sensor, but also solved the non-linear error caused by the eccentricity phenomenon of the FBGs as well as the machining deviation of the circular ring.

The designed pressurized FBG static level was composed of two parallel FBGs, circular structure, diaphragm, rigid rod, inlet, outlet and metal case. The schematic diagram in the static level was shown in Fig.1. The transmitting path of FBG static level was that when the water filled the whole case, the level pressure on the diaphragm was transmitted to the circular ring by the rigid rod. The compression of the ring in the vertical direction caused a positive strain in the lateral direction, which led to the shift of FBG central wavelength λ . The wavelength shift $\Delta\lambda$ was monitored to determine the change in settlement of measured points relative to the reference.

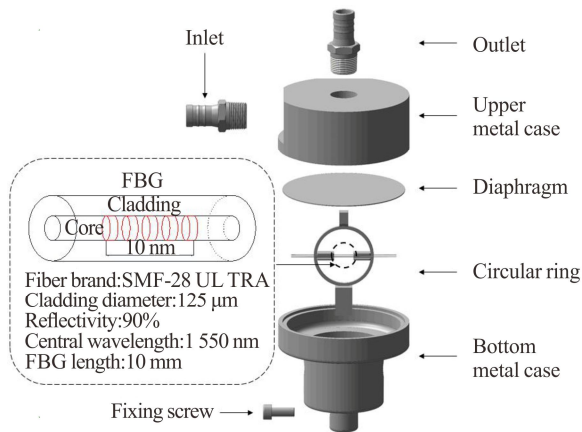


Fig.1 Schematic diagram of profile in FBG static level

The circular ring was the sensitive element in the FBG

static level. The sketch of its structure was shown in Fig.2. Moreover, suppose r was the radius of the circular ring. Suppose β was the angle between the line connecting the origin to each point on the circular ring and the y -axis. Since points A and C on the ring inside the sensor were connected to the diaphragm and the bottom of the metal case respectively, the level pressure sustained by the diaphragm was transferred to the points A and C of the ring in the concentrated force P . Meanwhile, the axial force N and bending moment M at each point of the circular section could be expressed as

$$N = \frac{P}{2} \cos \beta, \quad M = \frac{Pr}{2} \left(\cos \beta - \frac{2}{\pi} \right). \quad (1)$$

According to advanced mechanics of materials^[12], the differential equation of the deflection curve for the circular ring under the concentrated force P were

$$\begin{cases} \frac{d^2 v}{ds^2} = -\frac{v}{r^2} - \frac{M}{EI_z} \\ \frac{du}{ds} = \frac{v}{r} + \frac{N}{EA} + \frac{M}{EA r} \end{cases}, \quad (2)$$

where u , v , A and I_z denote the vertical displacement between A and C , horizontal displacement between B and D , cross-sectional area and moment of inertia of the circular ring, respectively. The length of the microelement on the ring satisfied $ds = r \cdot d\beta$. Substituting Eq.(1) into Eq.(2), the differential equation of the horizontal displacement for the ring with regard to v was obtained:

$$\frac{d^2 v}{d\beta^2} + v + \frac{Pr^3}{2EI_z} \left(\cos \beta - \frac{2}{\pi} \right) = 0. \quad (3)$$

The operator $d^2 v/d\beta^2$ in Eq.(3) satisfying both the conditions of self-association and linearity could be solved by the Ritz method. Firstly, the functional variation of the above equation was constructed.

$$\delta \Pi(v) = \int_{\Omega} \delta v \left[\frac{d^2 v}{d\beta^2} + v + \frac{Pr^3}{2EI_z} \left(\cos \beta - \frac{2}{\pi} \right) \right] d\Omega, \quad (4)$$

where the functional integral Π of Eq.(4) was

$$\Pi = \int_{\Omega} \left[\frac{vPr^3}{2EI_z} \left(\cos \beta - \frac{2}{\pi} \right) - \frac{1}{2} \cdot \frac{d^2 v}{d\beta^2} \right] d\Omega. \quad (5)$$

The determined coefficient δ was supported, and the trial function $v = \delta \cos 2\beta$ was chosen. When they were substituted into Eq.(5), it could be expressed as

$$\Pi = \int_0^{\pi/2} \left[\frac{Pr^3 \delta \cos 2\beta}{2EI_z} \left(\cos \beta - \frac{2}{\pi} \right) + 2\delta \cos 2\beta \right] d\beta = \frac{2Pr^3 \delta}{3EI} - \frac{3\pi \delta^2}{2}. \quad (6)$$

The determined coefficient δ containing within the functional integral was total differential that was made to be 0.

$$\frac{\partial \Pi}{\partial \delta} = \frac{2Pr^3}{3EI} - 3\pi \delta = 0. \quad (7)$$

From the above formula, the determined coefficient δ could be found as

$$\delta = \frac{2Pr^3}{9\pi EI} \tag{8}$$

Combining with the trial function, the horizontal displacement v between points B and D of the circular ring under the loading of the concentrated force P could be solved as

$$v = 2v|_{\beta=\pi/2} = -\frac{4Pr^3}{9\pi EI} \tag{9}$$

where the negative sign indicated that points B and D moved along the direction of deviation from the circular center. According to the symmetry of the circular structure, the corresponding vertical displacement between points A and C could be expressed as $u=-v$.

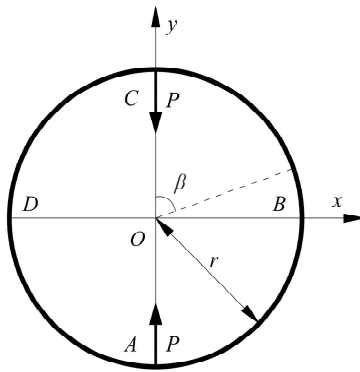


Fig.2 Analytical diagram of circular ring

The function of level pressure above the diaphragm sustaining the FBG static level was defined as $q(z)=\rho gz$. Subject to the uniform load $q(z)$, the deflection at the center of the circular diaphragm was solved as^[13]

$$w_q(z) = \frac{3q(z)(1-\mu^2)R^4}{16Et^3} \tag{10}$$

where R and t were the radius and thickness of the circular diaphragm within the FBG static level, as well as E and μ were the Young's modulus and Poisson's ratio of the material, respectively.

As shown in Fig.1, the rigid rod and circular ring existed in the following part of the circular diaphragm in the sensor. Rigid rod and circular ring would prevent the diaphragm to deform when the level pressure was loaded on the diaphragm. The mechanical model could be simplified as the central part of the diaphragm with a concentrated force F . Thus, the deflection of the diaphragm could be expressed as follows^[13]

$$w_F = \frac{3FR^2 \cdot (1-\mu^2)}{4\pi Et^3} \tag{11}$$

Assuming infinite rigidity of the rigid rod to ignore its axial deformation, the deflection at the center of the diaphragm under the joint loading of the level pressure $q(z)$ and the concentrated force F could be expressed as

$$w(z) = w_q(z) - w_F \tag{12}$$

The deformation-coordination equation of the FBG static level was $u=w(z)$. Furthermore, combining

Eqs.(9)—(12), the relationship between $q(z)$ and v could be obtained as

$$v = \frac{3\rho gzR^4 \cdot (1-\mu^2)}{16Et^3 \cdot [1 + \frac{27R^2I \cdot (1-\mu^2)}{16t^3r^3}]} \tag{13}$$

The elastic-optic coefficient of the optical fiber was defined as P_e . The variation of strain $\Delta\varepsilon$ as well as temperature ΔT caused a shift of the FBG central wavelength λ . The relation for the variation of its deflection $\Delta\lambda$ with considering only the external strain change was

$$\frac{\Delta\lambda}{\lambda} = (1 - P_e)\Delta\varepsilon \tag{14}$$

Therefore, the wavelength shift of the FBG which was pasted on the points B and D of the circular ring could be expressed as

$$\Delta\lambda = (1 - P_e)\lambda \frac{v}{l} = \frac{(1 - P_e)\lambda \cdot 3\rho gzR^4 \cdot (1-\mu^2)}{16Et^3 \cdot [1 + \frac{27R^2I \cdot (1-\mu^2)}{16t^3r^3}] \cdot l} \tag{15}$$

where l was the length of the FBG. Since the two FBGs were pasted to the lateral axis of the circular ring, the sensitivity S of the sensor could be expressed as

$$S = \frac{2 \cdot \Delta\lambda}{z} = \frac{(1 - P_e)\lambda \cdot 3\rho gR^4 \cdot (1-\mu^2)}{8Et^3 \cdot [1 + \frac{27R^2I \cdot (1-\mu^2)}{16t^3r^3}] \cdot l} \tag{16}$$

The metal material of the static level was selected from 316 steel to ensure its long-term reliability. The initial wavelength value of FBG was 1 550 nm. The dimensions of the sensitive element for the sensor were shown in Tab.1, substituting into Eq.(16) to obtain a theoretical sensitivity value of 6.08 pm/mm.

Tab.1 Relevant dimensions of the sensitive element

Element	Symbol	Meaning	Value (mm)
Diaphragm	R	Radius	20
	t	Thickness	0.5
Circular ring	r	Radius	10
	l	FBG length	6.8
Rigid rod	c	Length	5

To further illustrate the accuracy of the theoretical model based on the Ritz method for the FBG static level, the finite element software ABAQUS and static experiments were used to validate it. In the simulated analysis, FBG, circular structure and diaphragm were selected as beam element, solid element and plate element in the sensor, respectively. Since the major role of the metal case in the sensor was to transmit the level pressure with constraining the circular ring, the boundary conditions were set as fixed constraint at point C of the circular ring and the circumference of the diaphragm. The output result showed the wavelength variation of the two FBGs under the loading of 0—500 mm level height with an

interval step of 50 mm.

The *X*-direction displacement diagram of the sensitive element at full scale was shown in Fig.3. The uniform deformation of each element in the figure illustrated the reasonable setting of the dimensions in Tab.1. The diaphragm was deformed in concert with the circular ring under the action of level pressure, which in turn caused positive strain of the FBG. According to Fig.3, the simulated sensitivity of 4.84 pm/mm could be obtained by substituting the *X*-direction displacement of two points from the pasted FBG into Eqs.(14) and (16) in turn.

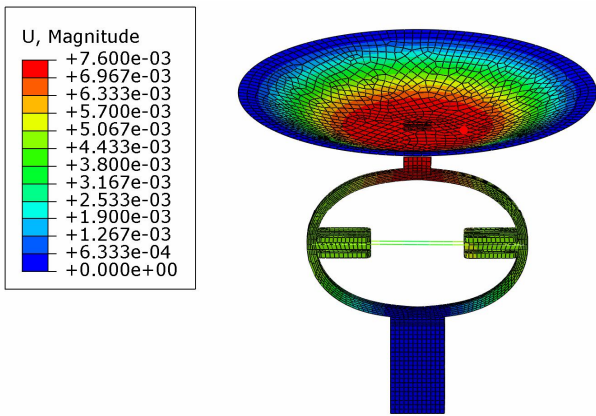


Fig.3 Displacement diagram of FBG static level

It could be found that there was a certain error between theory and simulation. That was because the stiffness at the position where the circular ring was connected to the rigid rod as well as the guide slot was much stiffer than the other positions on the ring. Fig.3 showed that the above-mentioned positions didn't produce the corresponding deformation. Whereas in Eq.(9) of the analysis, $\beta=90^\circ$ indicated that the circular ring was assumed above to be fully involved in the deformation. The deformation of the above position was assumed to be zero. The arc lengths of the connection between the ring and the upper rigid rod, the connection between the ring and the lower rigid rod as well as the connection between the ring and the fiber guide slot were defined as s_1 , s_2 and s_3 , respectively. The circumference of the ring was $2\pi r$. We defined the part of the ring which was involved in the deformation of the structure as the effective perimeter D . Combining the above symbols, the angle β as a function of radius r could be expressed as

$$\beta = \frac{D \cdot 90^\circ}{2\pi r} = \frac{2\pi r - s_1 - s_2 - 2s_3}{2\pi r} \times 90^\circ. \quad (17)$$

According to the dimensional design of Tab.1, s_1 , s_2 and s_3 in the sensor were similarly set to 3 mm. Combined with a circular radius r of 10 mm, $\beta=72.8^\circ$ was obtained, with the theoretical sensitivity of 4.99 pm/mm. It had an error of only 2.1% with the simulated sensitivity, which verified the accuracy of the Ritz method. Modified theoretical sensitivity was slightly higher attributed to the weakening influence of FBG not considered in the displacement analysis with Eq.(13).

The experimental test system mainly consisted of FBG static level, reservoir, OP-FBG 500 fiber grating demodulator and computer. The wavelength resolution of the demodulator was 0.1 pm while the sampling frequency was set to 50 Hz. The loading method involved using a measuring cylinder to fill the reservoir with water in which the wavelength shifts of two FBGs were recorded, while a syringe was used to draw up a quantitative amount of water for unloading. This operation inevitably caused the sensor to shake, so it was necessary to hold the sensor for 2 min after each loading or unloading before the next operation. Meanwhile, the threshold filtering algorithm was employed to process the initial wavelength data to reduce its burr phenomenon. The range and step settings of the loading experiment were consistent with the simulation, which was repeated three times in a cycle. In addition, the air remaining in the case must be removed using the outlet of the sensor before the experiment. The central wavelength values of two FBGs currently were 1 550.836 0 nm and 1 551.125 0 nm, respectively.

The time history plot of the FBG wavelength value was shown in Fig.4, which exhibited a step-wise transformation during cyclic loading. The variations of FBG1 and FBG2 during loading and unloading were similar in magnitude, indicating that they were perfectly sensitive to the deformation of the circular ring with a satisfactory pasting process. In addition, the high response rate of the sensor demonstrated that it could effectively identify settlement and uplift of structural engineering. The wavelength shifts of both FBG1 and FBG2 with respect to the initial value were summed, while the repeatability error of the sensor was only 1.29% as well as the hysteresis error of 1.17% based on the results of three replicated experiments.

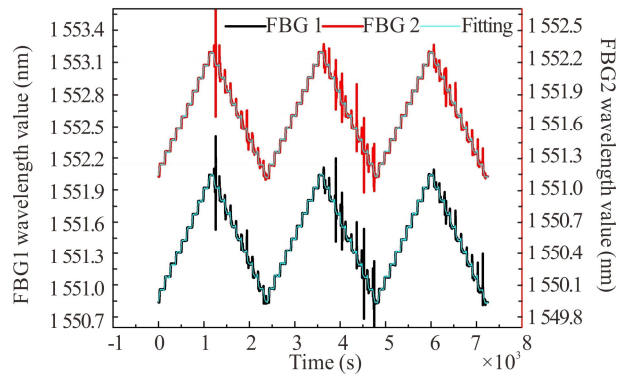


Fig.4 Wavelength variation of two FBGs

Comparing the theoretical analysis, finite element simulation and experiment, the wavelength shifts at level heights from 0 to 500 mm were shown in Fig.5. The experimental data were fitted based on the ordinary least square method where the sensitivity of the designed FBG static level was 4.75 pm/mm within the range with a linear correlation reaching 0.999 9. It could be found that

the experimental value was low, most notably owing to the strain transfer efficiency of 100% assumed both in theory and simulation in this paper. Since the OP-FBG 500 demodulator delivered a wavelength resolution of 0.1 pm, the resolution of the sensor in theory could be expressed as $0.1/4.75 \approx 0.02$ mm.

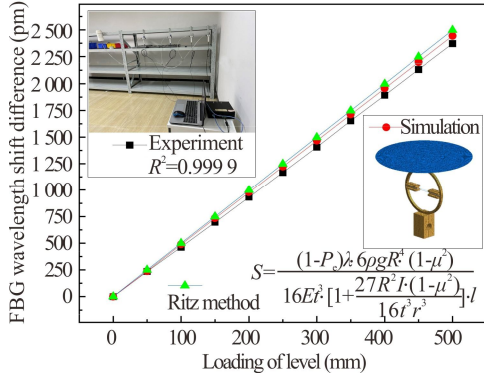


Fig.5 Sensitivity comparison of FBG static level

FBG and stainless steel 316 had sensitive response to environmental temperature. The FBG static level and a segment of unencapsulated FBG were placed in a temperature control box at the same time, where the wavelength shift of the FBG was recorded when the temperature was stable. The experimental temperature of the temperature control box was increased from 10 °C to 70 °C in 10 °C intervals. The experimental data of the sensor temperature were shown in Fig.6. The linear fitting showed that the temperature sensitivity of the ordinary FBG was 10.8 pm/°C, while the temperature sensitivity of the two FBGs in the static level was 24.5 pm/°C. It meant that the effect of the sensor on the variation of external temperature reached 49 pm/°C. Its temperature effect must be considered for correcting the negative influence of temperature sensitivity on the measured settlement. The solution to the temperature cross-sensitivity problem was achieved by taking the data of the measured points subtracted from the reference points. A complete connecting vessel system for settlement deformation consisted of reservoir, multiple FBG static levels, optical fiber cables, water pipes, and FBG demodulator. When monitoring the settlement at various points on the structure, a reference point for settlement as far away as possible must be installed. The measured value of the remaining FBG static levels should be subtracted from the reference point, thus avoiding the variation of settlement caused by factors such as evaporation of water. Encouragingly, the response in temperature of the measured points and the reference point were consistent when they were in the same gradient of temperature variation. When the data of the FBG static levels as the measured points were subtracted from the reference point, the effect of temperature sensitivity was avoided successfully, achieving temperature compensation in commercial application.

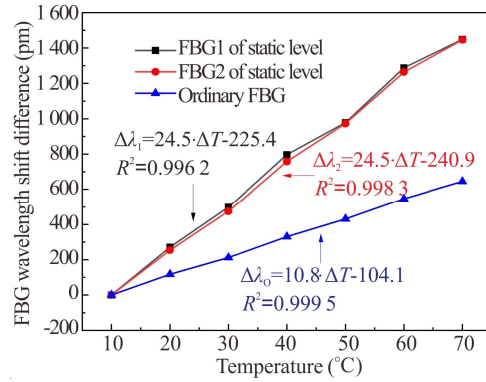


Fig.6 Temperature experiment of FBG static level

Taking an engineering project as an example, the monitoring requirement was to measure the long-term settling deformation of four bridge piers on soft ground. The designed FBG static levels were installed on the bridge piers as monitoring points, which were defined as 1#, 2#, 3# and 4#. The location of bridge abutment was used as the reference point, which was defined as 0#. The settling value of *i*# bridge pier was set as u_i . Combining with the 0# reference point, the settling variation Δu_i of *i*# bridge pier could be expressed as

$$\Delta u_i = u_i - u_0 = \frac{(\lambda'_{1,i} + \lambda'_{2,i}) - (\lambda_{1,i} + \lambda_{2,i})}{S_i} - \frac{(\lambda'_{1,0} + \lambda'_{2,0}) - (\lambda_{1,0} + \lambda_{2,0})}{S_0}, (i = 1, 2, 3, 4), \quad (18)$$

where $\lambda'_{1,i}$ and $\lambda'_{2,i}$ were the real-time wavelengths of FBG1 and FBG2 of *i*# pier respectively, as well as $\lambda_{1,i}$ and $\lambda_{2,i}$ were the initial wavelengths of FBG1 and FBG2 of *i*# pier respectively. By substituting the real-time measured wavelength data from the sensor on February 28th, 2021 into Eq.(18), the settlement curves of the four bridge piers on that day could be obtained. As shown in Fig.7, the threshold filtering algorithm was applied to process the data to obtain the smoothed settlement curve, which was indicated by the black line.

Settling deformation was a long-term cumulative evolution. Without structural damage to the bridge piers, excessive settling deformation was generally unlikely to occur in the short-term. On February 28th, 2021, we could consider that all the wavelength variations of the FBG static level were caused by the environmental temperature change, which were not related to the settlement. Analyzing the curve in Fig.7, it was noticed that by the zero o'clock of the second day, the settling values largely coincided with the zero o'clock of the first day. The phenomenon illustrated that the measured points subtracted from the reference point could eliminate the temperature shift effect to achieve compensation. In addition, the settling data in the early morning period of the day were relatively stable compared to the other periods. Therefore, when analyzing structural settlement, the data from the early morning period could be extracted to

avoid the influence of factors such as vehicle-induced vibration. The effectiveness of the designed FBG static level in measuring the structural settlement was demonstrated.

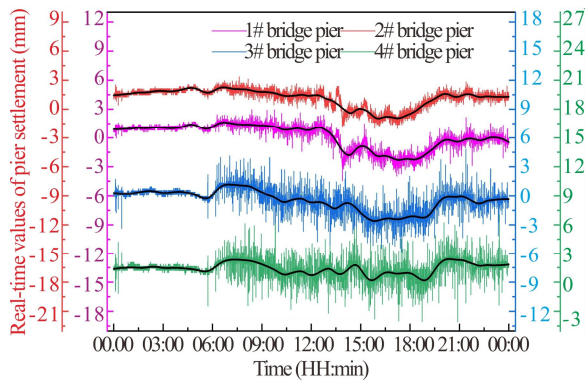


Fig.7 Real-time settling values of four bridge piers on February 28th, 2021

A novel pressurized FBG static level based on the structure of diaphragm and circular ring was designed in this paper, with the features of miniaturization, high sensitivity and minimal water evaporation. Combining the Ritz method with the deformation coordination equation, the theoretical sensitivity model of the sensor was established. According to the finite element results, the integration error of the circular structure was analyzed as well as corrected. Furthermore, the experiments on the sensitivity, repeatability and temperature through the sensor proved that the tests were in good agreement with the theoretical analysis. The linearity was up as high as 0.9999 while the temperature compensation function was achieved. Finally, the designed sensor was applied to settlement monitoring for bridge pier, whose measured result illustrated the advantages of the pressurized FBG static level used in bridge health monitoring.

Ethics declarations

Conflicts of interest

The authors declare no conflict of interest.

References

- [1] SIMUTIN A N, DEINEKO A V, ZERTSALOV M G. Experience of using the home-made monition automated hydrostatic-leveling system for monitoring of hydraulic structures[J]. Power technology and engineering, 2021, 55(4): 482-486.
- [2] HE Z X, ZHANG Z Y, LI L, et al. A novel fiber Bragg grating vibration sensor with double equal-strength cantilever beams[J]. Optoelectronics letters, 2021, 17(06): 321-327.
- [3] DIAZ C A R, LEAL-JUNIOR A, MARQUES C, et al. Optical fiber sensing for sub-millimeter liquid-level monitoring: a review[J]. IEEE sensors journal, 2019, 19(17): 7179-7191.
- [4] PEREIRA K, COIMBRA W, LAZARO R, et al. FBG-based temperature sensors for liquid identification and liquid level estimation via random forest[J]. Sensors, 2021, 21(13): 4568.
- [5] VORATHIN E, HAFIZI Z M. Bandwidth modulation and central wavelength shift of a single FBG for simultaneous water level and temperature sensing[J]. Measurement, 2020, 163: 107955.
- [6] RODRIGUES C, FELIX C, FIGUEIRAS J. Fiber optic-based displacement transducer to measure bridge deflections[J]. Structural health monitoring, 2011, 10(2): 147-156.
- [7] LIU W, WU X, ZHANG G, et al. Thin fiber-based Mach-Zehnder interferometric sensor for measurement of liquid level, refractive index, temperature, and axial strain[J]. Applied optics, 2020, 59(6): 1786-1792.
- [8] PABLO R V, ROSA P H, LUIS R C, et al. Liquid level sensor based on dynamic Fabry-Perot interferometers in processed capillary fiber[J]. Scientific reports, 2021, 11: 1-10.
- [9] PACHAVA V R, KAMINENI S, MADHUVARASU S S, et al. A high sensitive FBG pressure sensor using thin metal diaphragm[J]. Journal of optics, 2014, 43(2): 117-121.
- [10] AMEEN O F, YOUNUS M H, IBRAHIM R K R, et al. Comparison of water level measurement performance for two different types of diaphragm using fiber Bragg grating based optical sensors[J]. Jurnal teknologi, 2016, 78: 6-11.
- [11] LIU X B, LIANG L, JIANG K, et al. Sensitivity enhanced fiber Bragg grating pressure sensor based on a diaphragm and hinge-lever structure[J]. IEEE sensors journal, 2021, 21(7): 9155-9164.
- [12] UGURAL A C, FENSTER S K. Advanced mechanics of materials and applied elasticity[M]. London: Pearson Education, 2011.
- [13] KHAN S M, MISHRA R B, QAISER N, et al. Diaphragm shape effect on the performance of foil-based capacitive pressure sensors[J]. AIP advances, 2020, 10(1): 015009.